Microfluidic Devices Integrating Clinical Alternative Diagnostic Techniques Based on Cell Mechanical Properties

A. S. Moita(✉), D. Vieira, F. Mata, J. Pereira, and A. L. N. Moreira

IN+ - Center for Innovation, Technology and Policy Research,
Instituto Superior Técnico, Universidade de Lisboa,
Av. Rovisco Pais, 1049-001 Lisbon, Portugal
anamoita@tecnico.ist.utl.pt

Abstract. The present paper discusses the development of a microfluidic (lab-on-chip) device to study cells deformability aiming at developing a new diagnostic system for cancer detection. The chip uses electrowetting for droplet transport and cell deformability, on an open configuration. The chip configuration is analyzed towards various steps, from the selection of the materials, to the evaluation of the chip performance. Wetting properties of the selected materials are shown to play a major role. Furthermore, experimental tests confirm the relevance of selecting materials less prone to adsorb the biocomponents, as they tend to locally alter the surface wettability, promoting energy dissipation at the droplet contact line and affecting its manipulation. A rough analysis on droplet evaporation effects suggests that they are not negligible, even at optimum working conditions that minimize the evaporation by mass diffusion (low temperatures and high relative humidity). In this context, exploitation of droplet based microfluidic devices for point-of-care diagnostics in harsh environments should take mass diffusion effects into account.

Keywords: Microfluidic device · Electrowetting · Biofluid droplet dynamics
Wettability · Cancer diagnostics · Cell mechanical properties

1 Introduction

Innovative diagnostic tools are vital for accurate, early and prompt identification of many diseases, which may save peoples' lives. The fast development of microfluidics opened a wide range of possibilities in developing point-of-care microfluidic devices working as diagnostic tools, the so-called lab-on-chips.

Lab-on-chip systems swiftly evolved since their introduction by Manz [1] and are now able to perform several programmed operations and biochemical analysis. One major potential application of these microfluidic devices is in point-of-care diagnostics, as they meet the various requirements identified by the World Health Organization for the development of diagnostic tools for infectious diseases at resource-limited settings, such as affordability, sensitivity, equipment free, robustness and portability [2]. Despite claiming the ability to develop such systems at very low prices (approximately one Euro), researchers working in this field recognize the need for further research, to

N. Peixoto et al. (Eds.): BIOSTEC 2017, CCIS 881, pp. 74–93, 2018.
https://doi.org/10.1007/978-3-319-94806-5_4

devise an effective system, prone to deliver the quick and accurate diagnostics required in developing countries [3]. An important issue is related to the ambient conditions which affect the fluid and therefore the samples transport. This issue, recently approached by Moita *et al.* [4] is discussed in detail in this paper.

A paramount part of lab-on-chips development concerns the successful manipulation and transport operations of the biosamples, which are mainly a matter of momentum, energy and mass transport at liquid-solid interfaces. To cope with this, two main streams were followed, namely the sample transport in microchannel-based continuous microfluidics and the droplet-based digital microfluidics [5]. Although the first has been widely explored in a large number of applications, there are still some limitations associated to these systems, such as the fact that the functionality is not generally reconfigurable after design and fabrication, limiting more flexible applications, the samples are difficult to access, the systems are difficult to clean and maintain, clogging is more likely to occur and numerous auxiliaries such as tubes, valves, pumps, among others, are usually required, thus increasing the complexity of these systems. In addition, the efficiency of the valves and pumps at the micro-scale is still quite low, turning these systems inefficient from the energetic point of view. Conversely, the digital microfluidics based on droplets solves many of these issues, but the accurate control of droplet dynamics is not yet well understood. Most of the droplet based systems use a closed configuration with two plates, working as electrode and counter electrode, respectively. Despite being stable, this configuration keeps some of the problems pointed at the devices using microchannels, such as the clogging, the access to the samples, among others. Alternatively, the open configuration systems have still some problems to overcome. In the EWOD – Electrowettng on dielectric, the electrodes are covered by a thin dielectric layer to avoid the occurrence of hydrolysis [6]. The dielectric material is often hydrophobic to promote the motion of the droplet. As the droplet is deposited on the surface, the liquid-solid-vapour interfacial tensions are in equilibrium, defining the angle formed between the tangent line at the droplet edge and the surface, the so-called equilibrium contact angle [7]. Upon applying an electric potential, the droplet acts as a capacitor and an electric force is generated at the liquid-solid-vapour interface, unbalancing the interfacial tensions and decreasing the contact angle. This mechanism is classically described by the Young-Lippmann equation [7, 8] and despite the basic principles of EOWD are grounded for many decades, as revised for instance by [9], various alternative models (e.g. [10, 11]) strive to explain some unclear phenomena such as the contact angle saturation (i.e. the limiting value of the angle bellow which it remains unchanged, independently of the imposed electric potential), which are not predicted by Young-Lippmann theory.

The EWOD is therefore strongly dependent on the electrochemical properties of the aqueous solutions of the droplets. However, information reported in the literature concerning the transport of biofluids is actually quite sparse. Sirivasan *et al.* [12] report the successful transport of physiological fluids. Also, several authors report the effective electrowetting-induced transport of proteins and DNA [13], but it is not clear which are the most suitable electrochemical properties of the fluids or the most important parameters governing biofluids transport and manipulation. Adsorption of the biocomponents on the dielectric substrate is also a problem that is not completely described yet. For instance, [14, 15] report high adsorption of biocomponents and

particularly proteins by substrate materials commonly used as dielectrics in EWOD configurations, e.g. Teflon (PTFE – Polytetrafluoroethylene). The strong affinity of materials such as PTFE for the passive adsorption of proteins has also been recently confirmed by Moita *et al.* [4], who report a local modification of the wettability, which affects droplet motion. Hence, the wetting properties of the dielectric layer with the aqueous solutions in use and the affinity for passive and active adsorption should be inferred at earlier stages of the design and configuration of the microfluidic devices. The dynamic behavior of the biofluids to be manipulated must also be studied *a priori*, to assure the design of an effective device.

Concerning the use of these microfluidic devices, they have been widely explored for DNA manipulation (using electrophoresis working principle) [5] and for biochemical analysis of proteins and similar biocomponents (e.g. [13]). Clinical diagnostics has been less explored, but few authors already report the development of lab-on-chips for the early diagnose of several blood diseases and even cancer [3]. However, they are all based on chemical biomarkers and, exception made to the device developed by Di Carlo's team [3], which can separate circulating tumor cells from the other blood cells, they often still require the previous separation of various components of the sample, following numerous and complex procedures.

Conversely, the device discussed in the present paper will exploit cell mechanical properties to be used for cancer diagnostics. In fact, many cellular functions depend on the mediation and regulation of stress, as well as on the elastic and viscoelastic properties of the cell membrane [16]. Change in cell stiffness is a new characteristic of cancer cells and different types of cancer cells depict similar stiffness [17–19]. Detailed research on cell deformation is therefore proposed in more recent literature to play a vital role towards the early diagnostics of malignancy. Within the various cancer types addressing similar stiffness characteristics, lung cancer, diagnosed by analysis of the cells present in pleural fluid, is a particularly interesting research topic, given the difficulty in distinguishing between healthy and cancer cells based on shape and morphology parameters and even on chemical biomarkers. Also, cytological analysis of pleural fluids is not always reliable and immunofluorescence assays demand for specific sample preparation [20].

2 Experimental Procedure

The experimental procedure described in this section addresses the various steps followed in the microfabrication of the chips, the protocol defined to characterize the chips performance (mainly focusing on the transport and manipulation section) and diagnostic procedures to characterize the wettability and infer on the adsorption of the biocomponents.

2.1 Microfabrication of the Chips

The microchips' configurations were modelled in SOLIDWORKS and converted to AutoCAD files to be manufactured at INESC-MN. Here, configurations, mainly composed by arrays of interdigitated electrodes were printed on a 0.6 μm aluminium

film by lithography and wet etch on a glass substrate with 102 × 45 mm^2 and 700 μm width. Finally, a thin film of a dielectric material was deposited on the chip assembly, without covering the contacts. The different configurations tested only vary in the electrodes width, w (between 120 and 1400 μm), being the numerous interdigitated coplanar electrodes displaced with a fixed distance between them, 2a = 60 μm. The length of the electrodes is 24 mm (Fig. 1a and b).

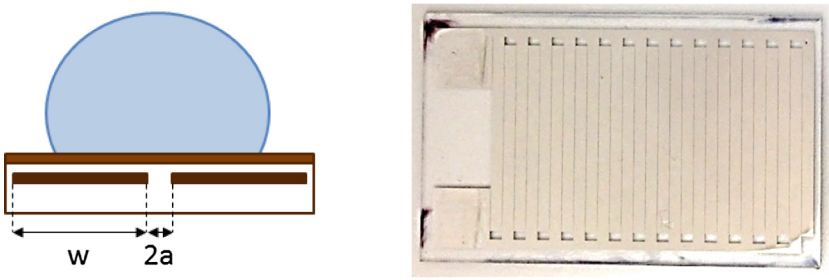

a) b)

Fig. 1. (a) Definition of the main geometrical parameters for the chip dimensioning. (b) Chip sample.

Since the coplanar electrodes have different polarities, the droplet must cover at least two electrodes. These basic dimensions were taken following the results obtained in the fundamental study previously completed [4]. Then, additional calculations on the chip capacitances and other electrical parameters were performed, following the recommendations of Chen *et al.* [21]. The best performing configurations were then selected empirically, based the analysis of the chips performance, as discussed in the following sections.

2.2 Preparation of the Biofluids and Characterization of Their Physico-Chemical Properties

The experiments are performed using a Green Fluorescent Protein - GFP (produced and purified in house) solution with 1.71 × 10^{-3} mM concentration and GFP-expressing E. coli suspensions with concentrations of 1 × 10^9 cells/ml and 2 × 10^9 cells/ml. The solutions and suspensions are characterized in terms of density, viscosity and surface tension. Density, ρ is measured with a pycnometer for liquids and the dynamic viscosity, μ with an ATS RheoSystems (a division of CANNON® Instruments, Co) under controlled temperature conditions. For the range of accuracy of ±5%, the solutions are observed to have density and viscosity values very close to those of water. Hence, all the solutions and suspensions are Newtonian fluids. Surface tension σ_{lv} is measured under controlled temperature conditions (20 ± 3 °C) with the optical tensiometer THETA (Attention), using the pendant drop method. The value taken for the surface tension of each liquid tested is averaged from 15 measurements. The surface tension of

Table 1. Physico-chemical properties of the solutions and suspensions used in the present work [22].

Solution	Density ρ [kg/m^3]	Surface tension σ_{lv} [mN/m]	Dynamic viscosity μ [Ns/m^2]
GFP (1.71×10^{-3} mM)	998	72.2 ± 0.7	1×10^{-3}
GFP-expressing E. coli (1×10^9 cells/ml)	998	73.8 ± 0.04	1×10^{-3}
GFP-expressing E. coli (2×10^9 cells/ml)	998	73.8 ± 0.04	1×10^{-3}

all the solutions used here is very close to that of water, as shown in Table 1, which summarizes the physico-chemical properties of the fluids used in the present work.

2.3 Measurement of the Contact Angles and Dynamic Response of the Biofluid Droplets: Evaluation of the Chips Performance

All experimental assays were performed inside a Perspex chamber with total dimensions of $55 \times 80 \times 90$ mm^3. This chamber has quartz windows to avoid optical distortion, which introduces errors in the image based techniques. The chamber was saturated with the working fluid and the tests were performed under continuous monitoring of temperature and relative humidity of the surrounding air. The measurements were taken with a DHT 22 Humidity & Temperature Sensor, at a sample rate of 0.5 Hz. Relative humidity was measured within 2–5% accuracy, while temperature measurements were taken within ±0.5 °C accuracy. The temperature was observed to be constant within T = 20 ± 3 °C and relative humidity was kept constant between 75% and 78%. Higher humidity values, up to 99% were then used to evaluate the effect of mass evaporation during the measurements.

The wettability of the dielectric substrates is quantified by the static contact angle θ_e and by hysteresis, determined as the difference between the quasi-static advancing and receding contact angles, measured with the optical tensiometer THETA from Attention. This characterization is performed for all the liquid-substrate pairs considered in the present study. The static angles are measured using the sessile drop method. The size of the images taken with the tensiometer is 640×480 pixels and the spatial resolution of the system for the current optical configuration is 15.6 μm/pixel. The images are post-processed by a drop detection algorithm based on Young-Laplace equation (One Attention software). The accuracy of these algorithms is argued to be of the order of ±0.1º [23]. Contact angle hysteresis is assessed at room temperature (20 °C ± 3 °C), following the procedure described by Kietzig [24]. Briefly, a small water drop is dispensed from a needle and brought into contact with the surface. The volume of the drop is increased and the advancing contact angle is taken as the one just before the interface diameter increases. Afterwards, the drop diameter decreases and the receding contact angle is taken as the one just before the interface diameter decreases. Given the relatively low resolution of these measurements obtained with an optical tensiometer and considering the typical scale of the processes governing the transport of the

samples within the droplets (micro-to-nano scale) and the paramount role of wettability, an alternative method is explored to provide more accurate measurements as proposed in Vieira *et al.* [25].

The performance of the chips is evaluated grounded on the dynamic response of the droplets on the chips, which in turn is discussed based on the evaluation of the temporal evolution of the droplet-surface contact diameter. The velocity of the contact line motion is also evaluated. These quantities are determined from high-speed visualization and post-processing. The high-speed images are taken at 2200 fps using a Phantom v4.2 from Vision Research Inc., with 512 × 512 pixels@2100 fps resolution. For the present optical configuration, the spatial resolution is 25 μm/pixel and the temporal resolution is 0.45 ms. The post-processing is performed using a home-made routine developed in Matlab. Temporal evolution of the contact (spreading and receding) diameters is presented as the average curve of at least 3 events, obtained at similar experimental conditions. Accuracy of the measurements is evaluated to be ±25 μm for the contact diameter.

Regarding the actuation of the chips, although AC voltage is reported by some authors to lead to better performances of the electrowetting systems, decreasing the contact angle hysteresis and delaying the contact angle saturation [10, 26] these phenomena seem to be more related to the wetting characteristics of the surfaces and with the properties of the solutions. Also, to avoid the occurrence of limiting frequencies for which the Lippmann equation is not satisfied [9], DC current was used on the chips provided by a Sorensen DCR600-.75B power supply. The applied voltage was varied from 0 to 245 V. However, since the basic principle for droplet motion in microchips requires switching polarities between neighboring electrodes, within an imposed frequency and following a similar approach explored by Fan *et al.* [27], a custom-made frequency controller using an Arduino was applied on the chips using a square wave, to assure the generation of an electrical force in the direction of the desired motion. This wave defines the time during which the electrode is actuated by a certain applied voltage. It has an internal clock with a frequency of 16 MHz. This device can vary the imposed frequency between 50 Hz and 400 Hz, within 50 Hz increments. The negative polarity of the chips was grounded, so, it will have a zero potential, i.e. the overall potential difference applied to the chip corresponds to the voltage applied to the positive polarity of the power supply.

2.4 Characterization of the Dielectric Substrates

To select the most appropriate dielectric substrates to be used, various coatings were tested, namely Teflon (PTFE), Polydimethylsiloxane (PDMS), SU8 resist and Silicon Nitrate (Si_3N_4). The coatings, chosen after extensive literature survey on the most used dielectric materials in EWOD are characterized based on their topography and on their static and dynamic wettability. Surface topography is characterized using a Dektak 3 profile meter (Veeco) with a vertical resolution of 20 nm. Within this resolution all the substrates are smooth. The contact angles are measured using the optical tensiometer THETA from Attention, as described in the previous paragraphs.

2.5 Adsorption Analysis Using Fluorescence Laser Scanning Confocal Microscopy

To infer on the possible adsorption of the biocomponents on the dielectric substrates, simple tests are performed in which droplets of 3.0 ± 0.2 mm of the biofluids (with different concentrations) are deposited on the surfaces. Afterwards, a sequence of tests with and without electrostatic actuation is performed and the "footprints" of the droplets are observed on a Laser Scanning Confocal Microscope (Leica SP8). The images are taken with a 4X magnification (0.10 of numerical aperture), with a pixel size of 5.42 μm × 5.42 μm. The obtained images are then post-processed to determine the mean grey intensity (sum of intensities divided by the number of pixels in the region of interest of the droplet footprint) and the Area Integrated Intensity (sum of intensities of pixels in the region of interest of the droplet footprint normalized by unit of area (μm^2). Since the droplet spreads after actuation, the integrated density is weighted with the area. To reduce the noise, the average grey intensity levels of the background image were also subtracted. The final result is the herein so-called Total Corrected Droplet Fluorescence – TCDF, as proposed by Moita *et al.* [4]. Higher values of TCDF can be associated to a larger quantity of protein or cells adsorbed by the substrate.

2.6 Contact Angle Measurements Using 3D Laser Scanning Fluorescence Confocal Microscopy

The 3D Laser Scanning Fluorescence Confocal Microscopy 3D LSFCM is an alternative diagnostic technique, developed as described in [25] which provides static and quasi-static contact angle measurements with high spatial resolution. The measurements were performed with a Laser Scanning Confocal Microscope (Leica TCS SP8), equipped with two lasers of continuous wave length. The maximum light power in the laser output is 350 mW and the excitation wave lengths available are 488 nm and 552 nm.

The measurements proceeded with the laser with 552 nm wavelength, set for the power of 10.50 mW (3.00% of the its maximum power) and gain of the photomultiplier (PMT) of 550 V. These values were set after a sensitivity analysis on the contrast of the image (before the post-processing) and on the Signal to Noise Ratio (SNR). The images are recorded in the format 1024 × 1024 and the scanning frequency is 400 Hz. In addition, the z-step was fixed in 1 μm for all the measurements.

A fluorescent dye - Rhodamine B (Sigma Aldrich) is used, which was chosen taken into account its excitation and emission wavelengths, to be compatible with the wavelengths available in the Laser Scanning Confocal Microscope, but also due to particular characteristics of the experimental conditions, in the present study. For the concentrations used here (0.0007936 mg/ml <Concentration <0.496 mg/ml) the physico-chemical properties of the water-dye solutions are very close to those of water.

While the resolution of the classical tensiometers and goniometers is of the order of tens to hundreds of microns, the pixel size achieved in this technique is, for the worse resolution 5.42 μm, but can be as small as 500 nm. Additional details on this technique can be found in [25].

To validate the 3D LSCFM technique, preliminary results were obtained by measuring the equilibrium contact angles on smooth glass slides. The equilibrium angles θ_{eq} are measured for millimetric and micrometric sizes, from 3 mm down to tens of microns. The measurements obtained are compared with those taken with the optical tensiometer. Various similar slides, from L1 to L4 are used to take into account the heterogeneities associated with material inhomogeneities and even surface defects. Hence, while Fig. 2 compares the equilibrium contact angles θ_e measured with the optical tensiometer with those obtained with the 3D LSFCM technique, for the same plane (XZ), Fig. 3, shows the dispersion of the measurements obtained for each technique, gathering in this case the measures obtained with the 3D LSFCM in 2 different planes (XY and XZ), to infer on possible asymmetries in the droplet shape. These asymmetries, which are not detected with the optical tensiometer are important for the application considered here, as they can distort the droplet and affect its motion in preferential directions.

Overall the results show that both techniques provide similar measurements, although the values obtained from the LSCFM tend to be slightly lower, when compared to those given by the optical tensiometer. This is due to the scale and resolution that are being considered in the LSCFM. The dispersion of the measurements is nevertheless quite similar in both techniques. Furthermore, the measurements in both XZ and YZ planes do not show an evident distortion of the contact line. Vieira *et al.* [25] report, however, significant distortions near the contact line region, when micro-structured surfaces are used. In such cases, the contact angles measured with the tensiometer can be up to 40º higher than those measured with the LSCFM technique, as these distortions affect the material contact angle (measured with the highest resolution) thus parting it from the apparent angle evaluated with the optical tensiometer. These observations of the contact line may also support our previous results (e.g. [4]) which showed that surface topography in these non-stable hydrophobic surfaces promotes energy dissipation at the contact line, thus precluding droplet motion. In line with these

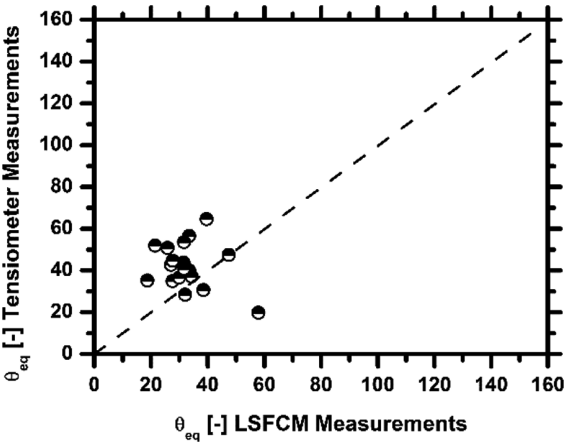

Fig. 2. Comparison between the equilibrium angles measured with the tensiometer and with the LSCFM technique, for a smooth glass surface. Adapted from [22].

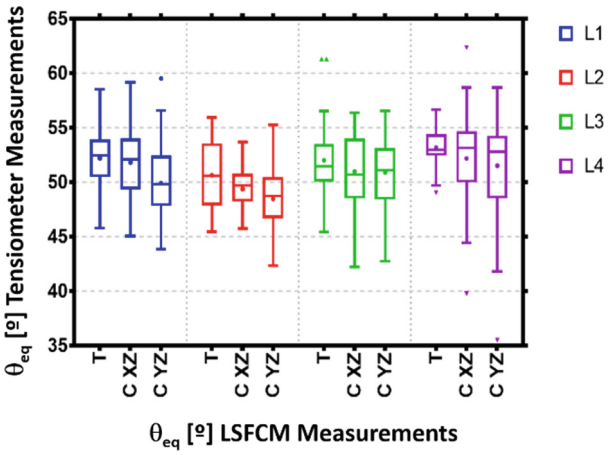

Fig. 3. Dispersion analysis of the static contact angles measured with the tensiometer and with the LSCFM technique, measured for smooth glass surfaces.

results, the safest way to alter wettability, avoiding the aforementioned issues, is towards the chemical modification and/or selection of the appropriate dielectric materials, as discussed in the following sub-section, while keeping the surface as smooth as possible.

3 Device Configuration

The microfluidic device under development has three main working sections, namely, the transport section, the diagnostic section and the selection section. The preferred wetting properties for the materials selected in each of these sections can be quite different. Hence, while in the transport section, droplet motion is governed by electrostatic actuation aided by custom made wetting properties of the dielectric material, so that hydrophobic/superhydrophobic regions are preferred to minimize the adhesive forces, which are proportional to hysteresis and consequently minimize the energy dissipated at the contact line between the droplet and the surface, in the diagnostic section it is desirable to promote adhesion to constrain the sample in the sensor area.

Hence and following the arguments presented in the Introduction, the wettability plays here a paramount role, so its characterization must be as accurate as possible. The materials, namely the dielectric material, which is in contact with the biosolutions, must therefore be chosen with care. For the transport and selection sections, the chosen materials should maximize the hydrophobicity with the fluids in study, minimize the hysteresis (to minimize the energy dissipation at the droplet contact line) and minimize

the adsorption, which locally affects the wettability, increasing the adhesion and, consequently the energy dissipation [4]. Opposite trends are desired for the diagnostics section. The various steps followed towards the selection of the materials is discussed in the following sub-section.

3.1 Selection of the Dielectric Substrates Based on Wettability and Adsorption Analysis

As aforementioned, the selection of the dieletric substrates is strongly dependent on their wetting properties. The analysis described in the next paragraphs was performed to select the materials to be used in the transport section. Similar reasoning was then followed for the diagnostic section, considering the specific requirements for this section, as previously discussed.

Hence, Table 2 depicts the equilibrium angles, obtained for each solution tested, on various dielectric coatings which are commonly used in electrowetting chips. Distilled and deionized water is taken as reference fluid. The Table shows that only the SU8 resist and Si3N4 surfaces are hydrophilic, being the others hydrophobic. The highest contact angle of 121º is obtained for the PDMS substrate. Low hysteresis is the complementary characteristic desired in the transport section. However, Fig. 4 shows that the materials depicting the highest contact angles with the working fluids, also depict large hysteresis of the contact angle. To cope with this, the best performing materials were further coated with Glaco®, a commercial coating which is mainly a perfluoroalkyltrichlorosilane combined with perfluoropolyether carboxylic acid and a fluorinated solvent. Its application allowed turning the substrates superhydrophobic to the aqueous solutions in study, portraying high contact angles (>150º) and low hysteresis (<10º), being therefore a good option to consider in the transport section of the microfluidic device. Following this analysis and taking into account the dielectric properties of these materials [28], PDMS and SU8 coated with Glaco® were the dielectric materials selected to coat the electrodes on the transport section.

Table 2. Equilibrium contact angles, obtained for each pair fluid-dielectric substrate considered in the present work [22].

Dielectric coating	Contact angle [°]		
	Water	*E-coli*	GFP
Teflon	112 ± 5	103 ± 6	121 ± 6
Teflon with Glaco	145 ± 1	141 ± 9	153 ± 3
PDMS	121 ± 1	112 ± 1	119.5 ± 0.4
PDMS with Glaco	153 ± 3	153 ± 2	155 ± 3
SU8 *resist*	67.1 ± 0.7	65 ± 2	71.8 ± 0.2
SU8 with Glaco	160 ± 7	162 ± 1	153 ± 4
Si_3N_4	64.1 ± 0.7	59 ± 4	65 ± 2

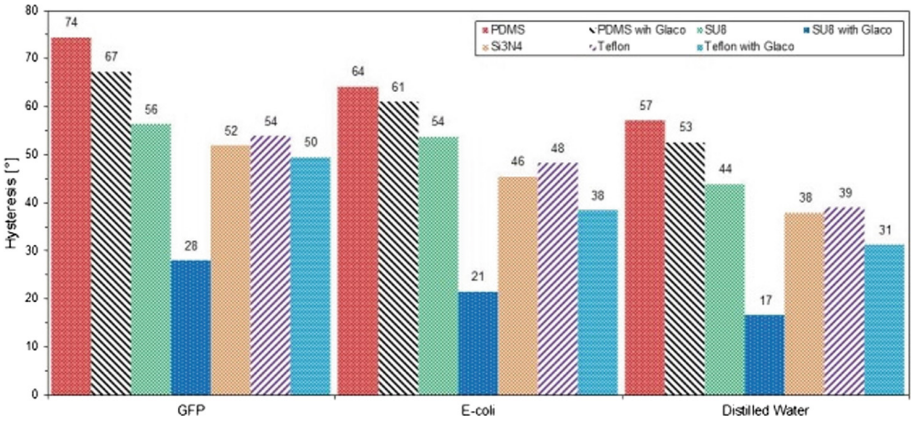

Fig. 4. Contact angle hysteresis evaluated for GFP solution (1.71×10^{-3} mM), GFP-expressing *E-coli* suspension (1×10^{9} cells/mL) and distilled water on the tested dielectric substrates [22].

Concerning adsorption, Moita *et al.* [4] report that the GFP was adsorbed by Teflon substrates, leading to a local increase of surface wettability and further contributing to preclude the receding motion, as this wettability increase is irreversible, taking the contact angles to values near saturation. In this context, the following analysis infers on the possible adsorption of the GFP and E-coli cells by the PDMS and SU8 substrates, as depicted in Fig. 5, which shows the TCDF value, as defined in Sect. 2, evaluated for each substrate.

Figure 5a evidences minimum TCDF values for the adsorption of the GFP on PDMS substrates. The alternative material with lower adsorption of the biocomponents tested here was SU8, but the TCDF values obtained are about one order of magnitude higher than those evaluated for PDMS. Even though the adsorption of cells is quite less significant than the adsorption of the protein, Fig. 5b suggests a minor effect of the cell concentration in the solutions in promoting passive adsorption mechanisms, i.e. leading to slightly higher TCDF values. Nevertheless, adsorption of E-coli cells was likewise observed to be minimum on the PDMS substrate. The application of the Glaco® coating is observed to further reduce the adsorption of both proteins and cells, decreasing the TCDF values in about one order of magnitude on the PDMS.

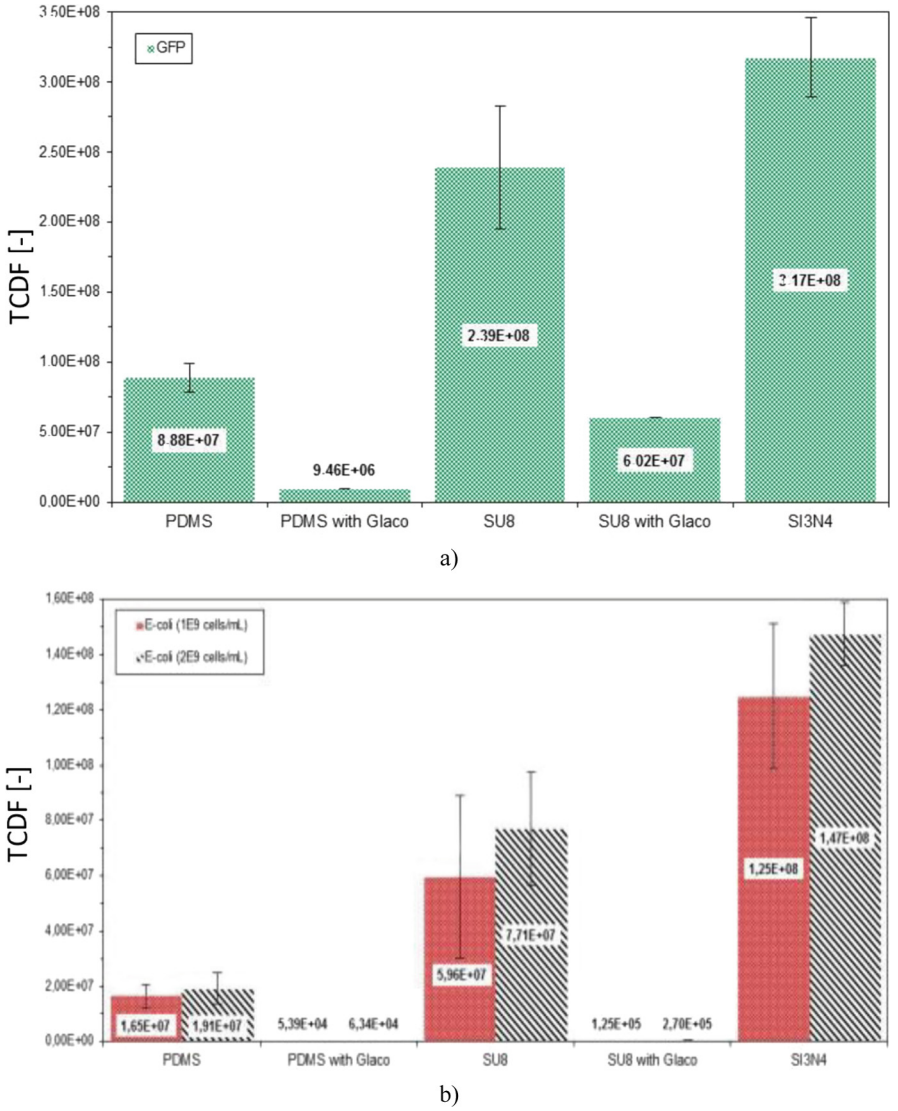

Fig. 5. Adsorption of the biocomponents (a) GFP and (b) E-coli cells by the dielectric substrates quantified by the TCDF.

3.2 Evaluation of the Chips Performance: Analysis of Influencing Parameters

After the selection of the materials, several chip configurations were tested, where the width of the electrodes was systematically varied. The best performing configurations were evaluated based on the dynamic response of the droplets, quantified by the droplet-surface contact diameter and by the velocity of displacement of the contact line.

This analysis determined that the best dynamic response was found for the chips with electrodes width w = 1200 μm and a distance between consecutive electrodes 2a = 60 μm. The detailed study performed is reported in [28].

The wetting properties have an important role in this dynamic response also, together with other parameters such as, for instance, the thickness of the dielectric layer, which is inversely proportional to the change in the contact angle during electrostatic actuation, as predicted by Young-Lippmann equation.

Hence, the spreading diameter of GFP and E-Coli suspension droplets, was evaluated under electrostatic actuation for the test chips coated with PDMS, SU8 resist and both materials further coated with Glaco®. As discussed in the previous sub-section, this coating reduces the adsorption of the proteins and of the cells by the substrates, so the irreversible contact angle decrease associated to the adsorption mechanisms is also minimized. The coating also decreases substantially the contact angle hysteresis. This modification of the wetting properties has a dramatic effect on the droplet transport on the chips, as shown in Fig. 6 which depicts the temporal evolution of the spreading diameter d(t) of a GFP droplet under electrostatic actuation, made non-dimensional with the initial diameter of the deposited droplet, i.e. for 0 V ($d(t)/d_{0V}$). t = 0 ms corresponds to the beginning of the actuation.

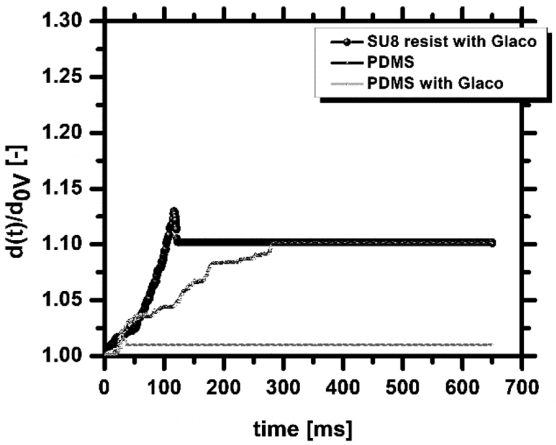

Fig. 6. Electrowetting induced spreading diameter of GFP droplets for different dielectric substrates, between coplanar electrodes for the configuration w = 1200 μm, at 230 V and 350 Hz. Initial droplet diameter is 2.8 mm.

The figure shows a significantly larger spreading diameter with the SU8 resist coated with Glaco®, being followed by a pronounced recoiling, allowed by the noteworthy hysteresis reduction. This recoiling will in turn allow the droplet to spread again towards the next electrode, in a continuous motion. The worse response of the droplet to the actuation obtained for PDMS coated with Glaco® is associated to the large final thickness of the substrate, which, according to Young-Lippmann equation,

precludes the decrease of the contact angle under actuation. Despite this reduced response, evident recoil is still observed.

However, as one looks at the overall maximum variation of the non-dimensional droplet diameter and of the velocity of the contact line, as a function of different imposed frequencies, the behavior of the droplet on the materials coated with Glaco® is not particularly improved in the sense that the droplet does not depict the largest diameters (Fig. 7a) or the highest velocities (Fig. 7b).

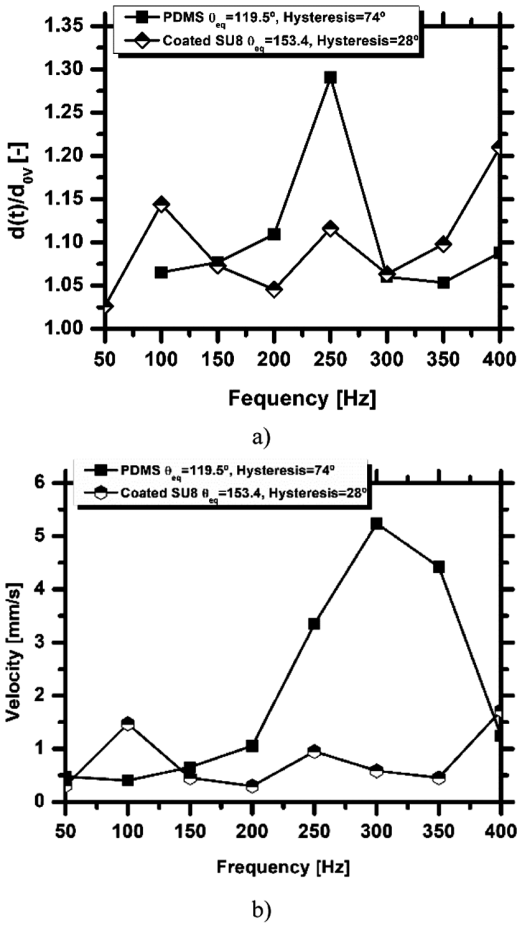

Fig. 7. Effect of the substrate wetting properties on the dynamic response of the droplets, namely on (a) the maximum spreading dimensionless diameter and (b) the maximum spreading velocities of GFP (1.71×10^{-3} mM) and GFP-expressing E-coli suspension (1×10^{9} cells/mL), for droplets moving between coplanar electrodes, for the configuration w = 1200 μm, for the configuration w = 1200 μm, 2a = 60 μm. Initial droplet diameter is 2.8 mm.

Once again, this result is attributed to the final thickness of the dielectric substrates, which precludes the actuation. Hence, the final device must be fabricated under strict control of the thickness of the dielectric layers used.

Droplet response is also affected by the nature and physico-chemical properties of the solutions. Figure 8 depicts the dimensional diameter and velocity of droplets of GFP and E-Coli solutions, as a function of the imposed frequency, for the same chip configuration used in the previous analysis.

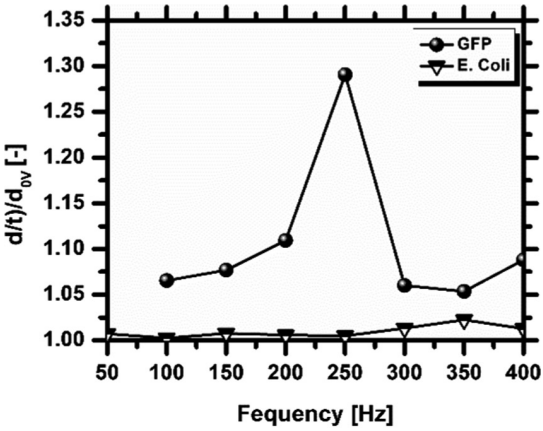

a)

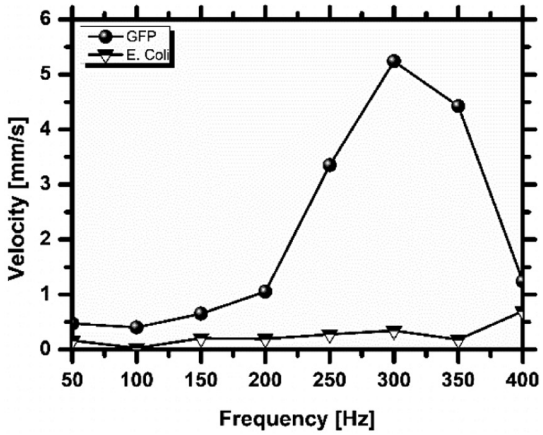

b)

Fig. 8. Effect of the solution composition on the dynamic response of the droplets, namely on (a) the maximum spreading dimensionless diameter [22] and (b) the maximum spreading velocities of GFP (1.71×10^{-3} mM) and GFP-expressing E-coli suspension (1×10^{9} cells/mL), for droplets moving between coplanar electrodes, for the configuration $w = 1200$ μm, $2a = 60$ μm. Initial droplet diameter is 2.8 mm.

The figure clearly shows the better response of the droplets of protein solutions, although the surface tension and density only vary slightly between the protein solution and the cell suspensions (Table 1). Hence, this particular behaviour is possibly attributed to local variations in the wettability or in the reorganization of the electrical density of the solution due to cell migration to the contact line region. However, this particular behaviour must be further studied in the near future, by characterizing the flow near the contact line.

3.3 Diagnostics Section

The diagnostic methodology to explore considers the correlation of different ratios of cell stiffness with the degrees of the pathology, being expected to be able to detect cell malignancy at very early stages [18]. Measurements of cell stiffness are usually obtained based on different separate methods (e.g. micro-pipetting, optical tweezers) and require specialized equipment such as Atomic Force Microscope and multiple preparation steps with extremely low output [29]. The work proposed here, on the other hand, addresses the full development of a microfluidic system to measure cell stiffness which does not require such complex equipment. Electrostatic actuation is explored aided by custom made surface wettability to achieve the required deformability ratios.

Cells stiffness is expected to be correlated with the deformation rates of the micro-droplets, which transport the samples. Isolated studies show the application of constitutive models [16] to explain cell stiffness. On the other hand, fluid dynamics research shows that the deformation behavior of even millimetric droplets is highly sensitive to the presence of microparticles or gums [30]. With the joined information, obtained from cell mechanics and flow dynamics, we will test the correlation between cell stiffness and microdroplets deformation. This will allow evaluating the feasibility of our approach.

3.4 Effects of Droplet Evaporation

As pointed in the Introduction, many authors argue for the potential of lab-on-chip devices for point-of-care diagnostics to be exploited for instance in developing countries. The ambient conditions however, can be a problem since to keep the device simple and affordable, there is not much room for the integration of complex systems to control the temperature and the relative humidity. These two parameters however, may strongly promote mass diffusion of the aqueous solutions, thus affecting the viability of the droplet based microfluidic system.

Based on a theoretical analysis, Moita et al. [4] report a non-negligible evaporation of a millimetric sessile droplet (30% of mass) within 1500 s of time intervals, for ambient temperatures of 23 $\pm$ 3 °C and a relative humidity of 70%. The evaporation rate of the droplets was also investigated in the present work, evaluating the temporal variation of the height and contact diameter of a sessile droplet, using the LSCFM technique.

To infer on the actual evaporation of the sample droplets, tests were carried out at experimental conditions similar to those reported in Moita *et al.* [4], although for a slightly lower ambient temperature (20 °C $\pm$ 2 °C). Temperature and relative humidity (HR) were monitored using the DHT 22 Humidity & Temperature Sensor. The measurements were performed inside the Perspex chamber, described in Sect. 2.

As discussed in the previous sections, after actuation, the droplet suffers in many cases an irreversible spreading process and the surface becomes locally hydrophilic. In a qualitative approach, under these circumstances, the evaporation of the droplet promotes the decreasing of the contact angle, while the wetting contact area remains approximately constant due to the pinning of the contact line [31].

Looking at our experimental results, in the assay performed at HR = 99.90% two stages can be identified (Fig. 9a): the first, where the liquid-solid contact area remains constant, as the contact angle decreases, in agreement with [31], transiting at t = 58.37 min for the second stage, where both the equilibrium contact angle and the contact area liquid-solid decrease. The height of the droplet decreases continuously over time (Fig. 9b).

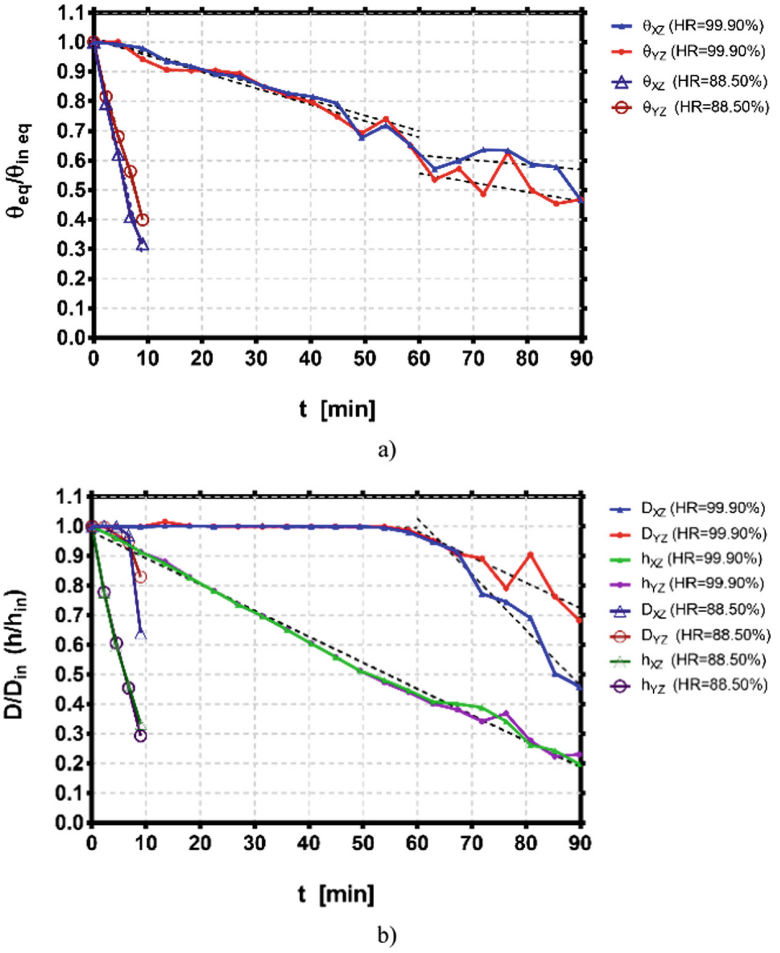

Fig. 9. Evaluation of droplet evaporation by mass diffusion. Temporal evolution of: (a) equilibrium contact angle and (b) droplet height and diameter, for the planes XZ and YZ of the droplet profile. D_{in} and h_{in} stand for the initial diameter and height of the deposited droplet, respectively.

The results further show that the contact angle decreases by about 53% of its absolute initial value. In addition, there is a reduction of the droplet height, evaluated in both planes XY and XZ, of approximately 80% in comparison to its initial height h_{in}. Also, the diameter of the deposited droplet decreases in 54% and 32% in planes XZ and YZ, respectively, compared to the initial values D_{in}.

For HR = 88.50%, the time resolution (2.25 min) is lower relatively to the HR = 99.90% assay (4.49 min) and does not allow identification of the two aforementioned evaporation states. Regarding the contact angle, a linear decrease of 68% and 60% is observed for the XZ and YZ planes, respectively – Fig. 9a.

Furthermore, the diameter of the contact area decreases by 36% (perspective XZ) and 17% (perspective YZ) in comparison to its initial value. In turn, the height decreases linearly throughout the whole period by roughly 67% of its initial height for both planes – Fig. 9b. These trends are qualitatively in agreement with those reported by Sobac and Brutin [32]. Quantitively, additional experiments must be performed to take more sustained conclusions. For instance, the relative humidity measurements require a more accurate evaluation within the entire chamber, since the evaporative rates are quite high, even for large values of HR, which may be associated to an actual global value of HR lower than that locally measured by the sensor. Despite this limitation, this rough evaluation indicates that the evaporation of the droplets is likely to occur even at controlled ambient conditions, so that a lab-on-chip system to be used in harsh environments (e.g. countries with high temperatures and dry climate) should address the possibility of a local increase of the HR inside the chip, for the time required for the analysis.

4 Conclusions

This paper addresses the development of a microfluidic (lab-on-chip) device integrating alternative diagnostic techniques based on cell stiffness and fluid rheological properties. Namely, the device exploits cell stiffness correlations with different stages of cancer. The samples are transported in microdroplets, manipulated by electrowetting, using an open configuration system.

The chip configuration is analyzed towards various steps and its performance in terms of droplet transport is evaluated based on the measurement of the droplet-surface contact diameter and of the displacement velocity of the contact line, which are observed to be affected by numerous parameters, such as the nature and composition of the biofluids used.

Wetting properties are also shown to play a major role in droplet manipulation.

Following this analysis, a model is now being developed to scale-down the devices, allowing to decrease the size of the droplets and consequently other parameters such as the imposed electric potential.

A rough analysis on droplet evaporation effects suggests that they are not negligible, even at controlled ambient conditions. Hence, lab-on-chip system to be used in harsh environments (e.g. countries with high temperatures and dry climate) should address the possibility of a local increase of the relative humidity inside the chip, for the time required for the analysis.

Acknowledgements. The authors are grateful to Fundação para a Ciência e a Tecnologia (FCT) for partially financing this research through the project UID/EEA/50009/2013, and for supporting D. Vieira with a fellowship. The work was also partially financed by FCT through the project RECI/EMS-SIS/0147/2012, which also funded the fellowships of F. Mata and J. Pereira. A.S. Moita also acknowledges the contribution of FCT for financing her contract through the IF 2015 recruitment program.

Finally, the authors acknowledge the contribution of Prof. Susana Freitas and her team from INESC-MN for the microfabrication of the test chips.

References

1. Manz, A., Widmers, H.M., Graber, N.: Miniaturized total chemical analysis systems: a novel concept for chemical sensing. Sens. Actuators B Chem. **1**(1–6), 244–248 (1990)
2. Yager, P., Edwards, T., Fu, E., Helton, K., Nelson, K., Tam, M.R., Weigl, B.H.: Microfluidic diagnostic technologies for global public health. Nature **442**(7101), 412–418 (2006)
3. Dance, A.: The making of a medical microchip. Nature **545**, 512–514 (2017)
4. Moita, A.S., Laurência, C., Ramos, J.A., Prazeres, D.M.F., Moreira, A.L.N.: Dynamics of droplets of biological fluids on smooth superhydrophobic surfaces under electrostatic actuation. J. Bionic Eng. **13**, 220–234 (2016)
5. Geng, H., Feng, J., Stabryl, L.M., Cho, S.K.: Dielectroetting manipulation for digital microfluidics: creating, transporting, splitting, and merging droplets. Lab Chip **17**, 1060–1068 (2017)
6. Berge, B.: Electrocapillarity and wetting of insulator films by water. Acad. Sci. Ser. II Mec. **317**, 157–163 (1993)
7. Young, T.: An essay on the cohesion of fluids. Phil. Trans. R. Soc. Lond. **95**, 65–87 (1805)
8. Lippmann, G.: Relation entre les phénomènes électriques et capillaires. Ann. Chim. Phys. **5**, 494–549 (1875). (in French)
9. Mugele, F., Baret, J.C.: Electrowetting: from basics to applications. J. Phys. Condens. Matter **17**, R705–R774 (2005)
10. Jones, T.B.: An electromechanical interpretation of electrowetting. J. Micromech. Microeng. **15**, 1184–1187 (2005)
11. Bahadur, V., Garimella, S.V.: An energy-based model for electrowetting-induced droplet actuation. J. Micromech. Microeng. **16**, 1494–1503 (2006)
12. Srinivasan, V., Pamula, V.K., Fair, R.B.: An integrated digital microfluidic lab-on-a-chip for clinical diagnostics on human physiological fluids. Lab Chip **4**, 310–315 (2004)
13. Wheeler, A.R., Moon, H., Kim, C.J., Loo, J.A., Garrell, R.L.: Electrowetting-based microfluidics for analysis of peptides and proteins by matrix-assisted laser desorption/ionization mass spectrometry. Anal. Chem. **76**, 4833–4838 (2004)
14. Rupp, F., Axmann, D., Ziegler, C., Geis-Gerstorfer, J.: Adsorption/desorption phenomena on pure and Teflon® AF-coated titania surfaces studied by dynamic contact angle analysis. J. Biomed. Mater. Res. **62**, 567–578 (2002)
15. Yon, J.Y., Garrell, R.L.: Preventing biomolecular adsorption in electrowetting-based biofluidic chips. Anal. Chem. **75**, 5097–5102 (2003)
16. Suresh, S., Spatz, J., Mills, J.P., Micoulet, A., Dao, M., Lim, C.T., Beil, M., Seufferlein, T.: Connections between single-cell biomechanics and human disease states: gastrointestinal cancer and malaria. Acta Biomater. **1**, 15–30 (2005)
17. Cross, S.E., Jin, Y.-S., Rao, J., Gimzewski, J.K.: Nanomechanical analysis of cells from cancer patients. Nat. Nanotechnol. Lett. **2**, 780–783 (2005)

18. Gosset, G.R., Tse, H.T.K., Lee, S.A., Ying, Y., Lidgren, A.G., Yang, O.O., Rao, J., Clark, A.T., Di Carlo, D.: Hydrodynamic stretching of single cells for large population mechanical phenotyping. PNAS **109**(20), 7630–7635 (2009)
19. Remmerbach, T.W., Wottawah, F., Dietrich, J., Lincoln, B., Wittekind, C., Guck, J.: Oral cancer diagnosis by mechanical phenotyping. Cancer Res. **69**(5), 1728–1732 (2009)
20. Tse, H.T.K., Gosset, D.R., Moon, Y.S., Masaeli, M., Sohsman, M., Ying, Y., Mislick, K., Adams, R.P., Rao, J., Di Carlo, D.: Quantitative diagnosis of malignant pleural effusions by single-cell mechanophenotyping. Sci. Transl. Med. **5**(212), 1–9 (2013)
21. Chen, J.Z., Darhuber, A.A., Troian, S.M., Wagner, S.: Capacitive sensing of droplets for microfluidic devices based on thermocapillary actuation. Lab Chip **4**(5), 473–480 (2004)
22. Vieira, D., Mata, F., Moita, A.S., Moreira, A.L.N.: Microfluidic prototype of a lab-on-chip device for lung cancer diagnostics. In: Proceedings of the 10th International Joint Conference on Biomedical Engineering Systems and Technologies - Volume 1: BIODEVICES, Porto, Portugal, 21–13 February 2017, pp. 63–68 (2017). https://doi.org/10.5220/0006252700630068. ISBN: 978-989-758-216-5
23. Cheng, P., Li, D., Boruvka, L., Rotenberg, Y., Neumann, A.W.: Automation of axisymmetric drop shape analysis for measurements of interfacial tensions and contact angles. Colloids Surf. **43**(2), 151–167 (1990)
24. Kietzig, A.M.: Comments on "an essay on contact angle measurements" – an illustration of the respective influence of droplet deposition and measurement parameters. Plasma Proc. Polym. **8**, 1003–1009 (2008)
25. Vieira, D., Moita, A.S., Moreira, A.L.N.: Non-intrusive wettability characterization on complex surfaces using 3D laser scanning confocal fluorescence microscopy. In: 18th International Symposium on Applications of Laser and Imaging Techniques to Fluid Mechanics, Lisbon (2016)
26. Chen, L., Bonaccurso, E.: Electrowetting - from statics to dynamics. Adv. Colloid Interface Sci. **210**, 2–12 (2014)
27. Fan, S.-K., Yang, H., Wang, T.-T., Hsu, W.: Asymmetric electrowetting–moving droplets by a square wave. Lab Chip **7**(10), 1330–1335 (2007)
28. Mata, F., Moita, A.S., Kumar, R., Cardoso, S., Prazeres, D.M.F., Moreira, A.L.N.: Effect of surface wettability on the spreading and displacement of biofluid drops in electrowetting. In: Proceedings of ILASS – Europe 2016, 27th Annual Conference on Liquid Atomization and Spray Systems, September 2016, Brighton, UK, 4–7 September 2016 (2016). ISBN 978-1-910172-09-4
29. Adamo, A., Sharei, A., Adamo, L., Lee, B., Mao, S., Jensen, K.F.: Microfluidics-based assessment of cell deformability. Anal. Chem. **84**, 6438–6443 (2012)
30. Moita, A.S., Herrmann, D., Moreira, A.L.N.: Fluid dynamic and heat transfer processes between solid surfaces and non-Newtonian liquid droplets. Appl. Therm. Eng. **88**, 33–46 (2015)
31. Picknett, R., Bexon, R.: The evaporation of sessile or pendant drops in still air. J. Colloid Interface Sci. **61**(2), 336–350 (1977)
32. Sobac, B., Brutin, D.: Triple-line behavior and wettability controlled by nanocoated substrates: influence on sessile drop evaporation. Langmuir **27**(24), 14999–15007 (2011)